COMPENSATING FOR THE FINITE SIZE OF SAR PROBES USED IN ELECTRIC-FIELD GRADIENTS

MI Manning, Indexsar Ltd.

Introduction

SAR probes with 3 diode-sensors in an orthogonal arrangement are designed to display an isotropic response when exposed to a uniform field. However, the probes are ordinarily used for measurements in non-uniform fields and isotropy is not assured when the field gradients are significant compared to the dimensions of the tip containing the three orthogonally-arranged dipole sensors.

It becomes increasingly important to assess the effects of field gradients on SAR probe readings when higher frequencies are being used. For Indexsar IXP-050 probes, which are of 5mm tip diameter, field gradient effects are minor at GSM frequencies, but are major above 5GHz. Smaller probes are less affected by field gradients and so probes, which are significantly less than 5mm diameter, would be better for applications above 5GHz.

In P1528, which covers frequencies up to 3GHz, Section 6.5.2 recommends that the probe axis should be oriented within 30 degrees to a line normal to the phantom surface to reduce probe boundary effects*:*

> *"If this angle is larger than 30 degrees and the closest point on the tip housing to the phantom surface is closer than a probe diameter, the boundary effect may become larger and polarization dependent. This additional uncertainty needs to be analyzed and taken into account, for which modified test procedures and additional uncertainty analyses not described in this recommended practice is required."*

This report describes theoretical and experimental studies to evaluate the issues associated with the use of probes at arbitrary angles to surfaces and field directions. Based upon these studies, the procedures and uncertainty analyses referred to in P1528 are addressed for the full range of probe presentation angles.

In addition, generalized procedures for correcting for the finite size of immersible SAR probes are developed. Use of these procedures enables application of schemes for virtual probe miniaturization (VPM) – allowing probes of a specific size to be used where physically-smaller probes would otherwise be required.

Given the typical dimensions of 3-channel SAR probes presently available, use of the VPM technique extends the satisfactory measurement range to higher frequencies.

Effect of sensor displacement from probe axis on spatial resolution

A measurement procedure is recommended in P1528 Section A.6.2 to investigate the effect of sensor displacement on spatial resolution. A sharp field minimum is introduced using parallel dipoles and the minimum is scanned using the probe. Such tests have been performed both at the side and the bottom of a box phantom using an Indexsar IXP-050 SAR probe. Details are given in Appendix 1. The results are similar at both the side and bottom of the box, but the response at the bottom of the box is smoothed out due to the displacements of the sensors in the field gradient direction. A sharper minimum is measured at the side of the box because the sensors are in the same plane as the field minimum. The results of this test demonstrate the potential for implementing procedures for compensating for sensor displacement.

email: enquiries@indexsar.com http://www.indexsar.com
Oakfield House, Cudworth Lane, Newdigate, Surrey, RH5 5BG, UK.

Theory of probe response in a field gradient

When a SAR probe is exposed to any field gradient that is not aligned with the probe axis, each of the 3 individual sensors will be in regions of different field strength. However, the position recorded for the probe is the mid-point of all three sensors. Thus the sensors further away will read low and those closer to the source will read high. The situation is further complicated because the sensors are set at an angle to the probe axis (of +/- 54.7 degrees if the theoretical angle is employed) so that sensor sensitivity varies with the direction of the field polarization and that of the sensor dipole. In this report, this situation is analyzed first for the geometry used for isotropy testing (Fig A.2 in P1528 [1]), and subsequently for the generalized situation where the probe can have any angle to the local field gradient.

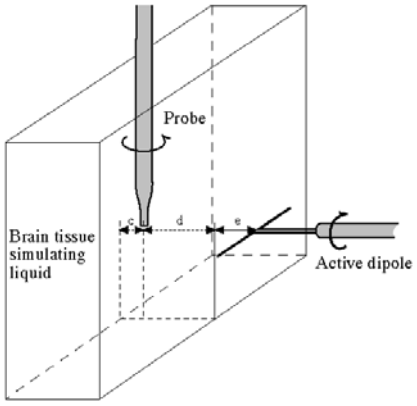

Figure 1: The test geometry illustrated in P1528 Figure A.2

The diagram below defines a coordinate framework and the angles of the source dipole and one of the sensor dipoles in the E-field probe.

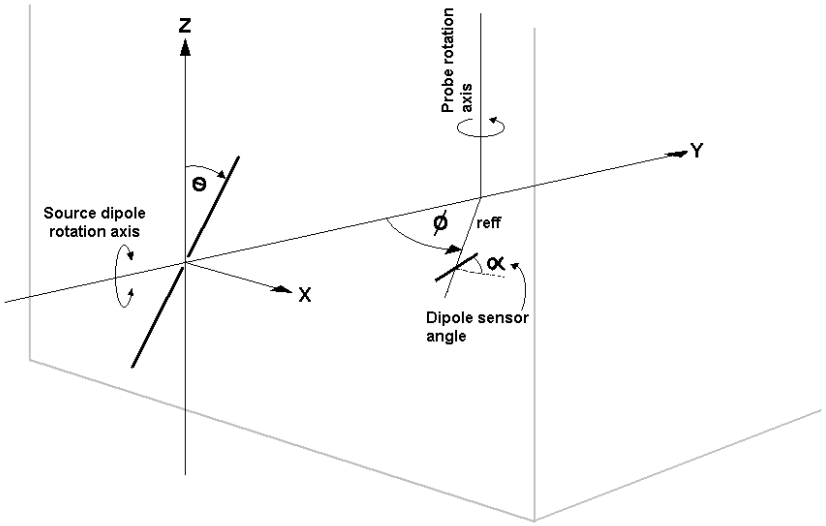

Figure 2: Coordinate system and angular reference points

In the Figure 2, θ is the angle of rotation of the source dipole with respect to the Z direction. Φ is the angle between the sensor location and the direction of the source. α is the sensor dipole angle from horizontal (this can be of either sign depending on the probe construction). r_{eff} is the effective sensor radius within the probe tip. Unit direction vectors for the source dipole and for the sensor dipole can be described as below

email: enquiries@indexsar.com http://www.indexsar.com
Oakfield House, Cudworth Lane, Newdigate, Surrey, RH5 5BG, UK.

source dipole unit vector: $X_d = \sin\theta$; $Y_d = 0$; $Z_d = \cos\theta$
sensor dipole unit vector: $X_s = \cos\Phi.\cos\alpha$; $Y_s = \sin\Phi$; $Z_s = \sin\alpha$

The sensor sensitivity is given by the cosine of the angle between them

$$\text{sensor sensitivity} = | X_d X_s + Y_d Y_s + Z_d Z_s |$$

$$= |(\sin\theta.\cos\Phi.\cos\alpha + \cos\theta.\sin\alpha)|$$

where the absolute value is taken since the sensor output is rectified. The magnitude of the local E-field also needs correction for position of the sensor down the field gradient

$$\text{distance correction} = e^{-r_{eff}.dr.\cos\Phi}$$

Where r_{eff} is the effective sensor radius, dr is the attenuation constant (= 1/ skin depth. See definitions in P1528 Section 3) and Φ is the sensor rotation from the source direction. For probe output which is (when linearised) proportional to E^2 or SAR,

$$\text{distance correction} = e^{-2.r_{eff}.dr.\cos\Phi}$$

The equations above allow us to calculate the variation of output of a diode sensor, U_{sensor} , with rotation angle

$$U_{sensor} = U_{centre} \, |(\sin\theta.\cos\Phi.\cos\alpha + \cos\theta.\sin\alpha)| \, e^{-2.r_{eff}.dr.\cos\Phi}$$

where U_{centre} is the value of the field at the centre of the probe tip

This equation can be used three times at angles 2π/3 apart to predict the isotropic response of a 3-channel probe in field gradients of different magnitude as shown in Figure 3.

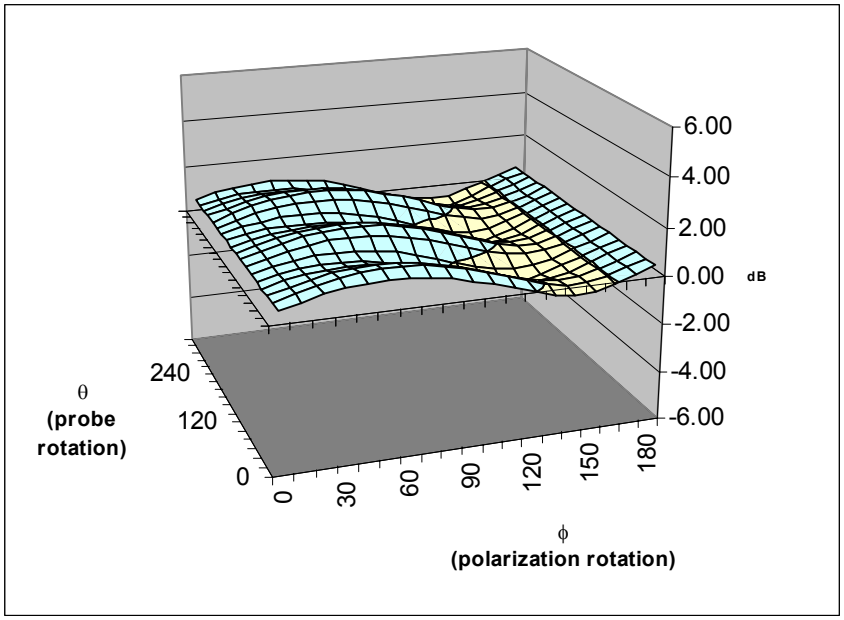

Figure 3: Predicted isotropic response of probe with an effective sensor radius of 1.25mm and a sensor angle of 35.3 degrees. The result shown is for a penetration depth of 9mm corresponding to 2450MHz box testing. The probe rotation is offset by 20 degrees to correspond with the measured data. The max. spherical isotropy range predicted is +/- 1.1227dB and the maximum rotational isotropy range is +/- 0.53 dB.

email: enquiries@indexsar.com http://www.indexsar.com
Oakfield House, Cudworth Lane, Newdigate, Surrey, RH5 5BG, UK.

The corrections require some knowledge of the direction and magnitude of the local field gradient. In this study, spot SAR measurements have been obtained and the frequency dependence of the magnitude of the field gradient can be deduced from related waveguide calibration measurements. However, the field decay rates in a waveguide (a unidirectional decay) are different from those in a box phantom, where field decays are omni-directional. In principle, 3D scanning measurements contain details of the field decay rate and of its direction, so an automated correction process can be implemented. Different levels of compensation procedure are considered below.

Uni-axial correction scheme for upright box phantom

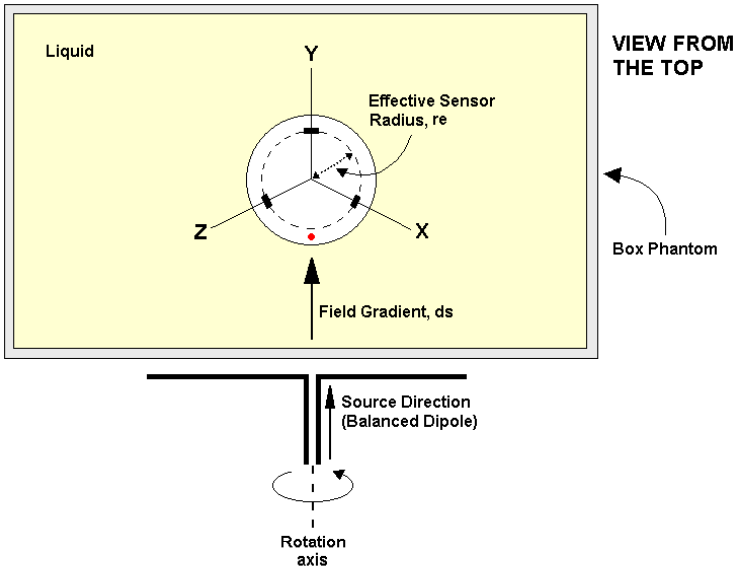

Figure 4: Illustration of the geometry for a uniaxial correction scheme.

With regard to Figure 4, which is looking down on a liquid-filled box phantom with a vertical probe, the probe outputs can be corrected by using the following equations:

$$X_c = X * EXP(-2\, r_{eff}\, dr\, COS(X_s))$$
$$Y_c = Y * EXP(-2\, r_{eff}\, dr\, COS(X_s + 2\pi/3))$$
$$Z_c = Z * EXP(-2\, r_{eff}\, dr\, COS(X_s + 4\pi/3))$$

where X_c is the corrected probe output, r_{eff} is the effective sensor radius, dr is the local decay rate as a factor per unit distance and X_s is the angle between the X sensor direction and the direction of source presentation (normal to the phantom).

email: enquiries@indexsar.com http://www.indexsar.com
Oakfield House, Cudworth Lane, Newdigate, Surrey, RH5 5BG, UK.

Tri-axial correction scheme for generalized 3D data sets
Given a set of 3D gridded measurement data and details of the probe presentation angle at each position, the field gradients can be evaluated at each position and corrections for the offsets of each sensor in the gradient direction can be applied.

To develop the required formalism, assume that the gridded data and the probe positioning share the same Cartesian co-ordinate system. Assume that the probe axis is constrained to pass through the point X=0, Y=0, Z=0. Then, if the probe is at a position X, Y, Z, the probe presentation angle is obtained very simply from the position. For example, the inclination in the X-plane is ATAN(X/Z) and so forth for the other inclinations.

Each of the three sensors will have an offset from the nominal measurement location in the X, Y and Z directions. So there are 9 offsets in all:

For the x sensor:

X offset of x sensor = r_{eff} COS(X_s). COS(ATAN(X/Z))
Y offset of x sensor = r_{eff} SIN(X_s). COS(ATAN(Y/Z))
Z offset of x sensor = r_{eff} (SIN(X_s). SIN(ATAN(Y/Z)) + COS(Xs).SIN(ATAN(X/Z)))

Similarly for the other sensors but using Xs + 2π/3 or Xs + 4π/3 as appropriate.

The correction factors that need to be applied to each sensor measurement are obtained from the offsets by multiplying them by the local field gradients at each point. To obtain the local field gradients, the 3D gridded data are processed using a software algorithm to make a new array of the gradients at each point. A suitable algorithm is given in Appendix 2. Importantly, in this scheme, it is **not** necessary to have prior knowledge of the field gradients as they are evaluated from the measured data. Also, knowledge of the field polarization direction is not required.

The correction process involves replacing the measured 3D arrays of data with corrected arrays and then continuing with the remaining data post-processing stages

Experimental isotropy measurements in field-gradients 835MHz- 5.8GHz
In this study, a SAR probe has been maintained vertically in a rectangular liquid-filled phantom to which a dipole source has been applied from the side. The dipole source has been rotated through rotations from 0 to 180 degrees (angle between dipole arm and probe axis). It is important to realize that it is not sufficient to rotate the source through only 90 degrees as only half the probe anisotropy will be captured. In the measurement process, the probe is thus exposed laterally to the maximum available field gradient whilst the source polarization angle is varied. Dipoles dimensioned according to recommendations in P1528 (Annex G) have been used for frequencies from 835MHz through 2450MHz. The dipole used for 5200 and 5800 MHZ was improvised from a 2450MHz dipole and was not made according to recommendations that have subsequently appeared in a draft annex (Annex X) to P1528 (Table X.5).

The uncorrected measurements from 835MHz to 2450Mhz obtained agree very well with the theory presented above. For example, Figure 5 shows experimental measurement data for comparison with the analytically derived response shown in Figure 3.

email: enquiries@indexsar.com http://www.indexsar.com
Oakfield House, Cudworth Lane, Newdigate, Surrey, RH5 5BG, UK.

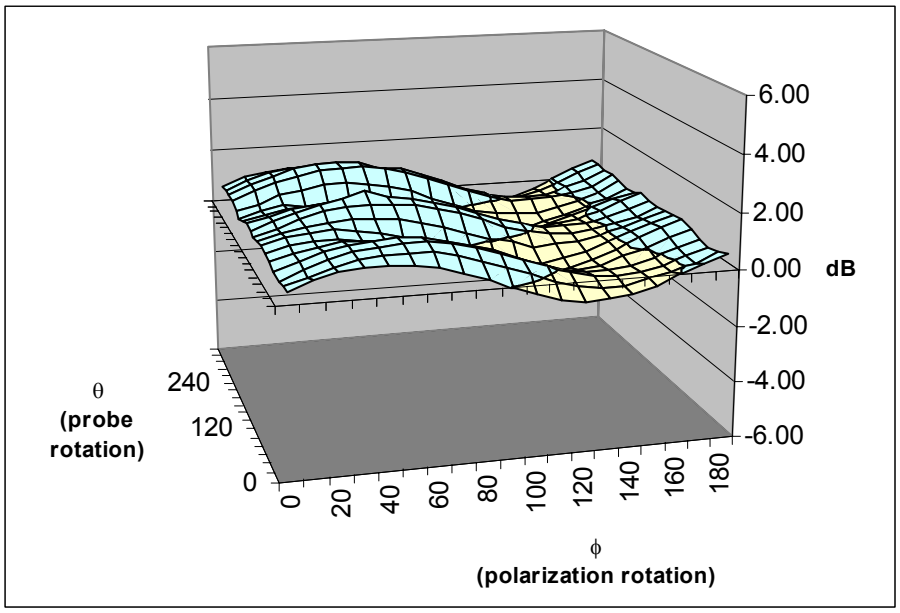

Figure 5: Measured isotropic response of an IXP-050 probe with tip diameter of 5 mm at 2450MHz. The probe rotation started with the X sensor at 20 degrees rotation to the source. The max. spherical isotropy range measured was +/- 1.136dB and the maximum rotational isotropy range was +/- 0.79 dB.

Measurement results were obtained at frequencies between 835MHz and 58000MHz and are shown graphically in Figures 6 – 9 below and summarized in Table 1. Corrections have been applied using the uni-axial procedure developed from the analytical equations. For these corrections, an effective sensor radius of 1.25mm was used in all cases and the penetration depth in the box for optimum corrections is as shown in brackets in Table 1 column 5. Box penetration depths would be expected to be somewhat less than for a uni-directionally dispersing wave in a waveguide.

email: enquiries@indexsar.com http://www.indexsar.com
Oakfield House, Cudworth Lane, Newdigate, Surrey, RH5 5BG, UK.

Table 1: Results - Spherical isotropy range versus frequency

Frequency (MHz)	Max. anisotropy in field gradient – uncorrected (+/- dB)	Max. anisotropy corrected for field gradient (+/- dB)	Rotational isotropy in field gradient (+/- dB)	Penetration depth (E) from waveguide decay meas. (and in box) (mm)	IXP-050 Probe S/N
835	0.464	0.368	0.22/0.14	49.0 (36)	0084
900	0.542	0.330	0.28/0.17	34.9 (28)	0084
1800	0.884	0.556	0.57/0.31	24.0 (11)	0084
2000	1.323	0.705	0.86/0.32	20.0 (10)	0084
2450	1.136	0.789	0.79/0.44	18.0 (9)	0084
5250	3.111	1.023	1.85/0.83	5.73 (4)	0125
5800	3.293	1.014	2.07/0.94	5.25 (4)	0125

Table 2: Dielectric properties for the liquids used in the box phantom tests at each frequency

Frequency (MHz)	Relative permittivity	Conductivity (S/m)
835	42.9	.89
900	42.5	.97
1800	39.50	1.74
1900	38.77	1.86
2450	35.10	2.45
5250	43.60	6.3
5700	40.09	6.6

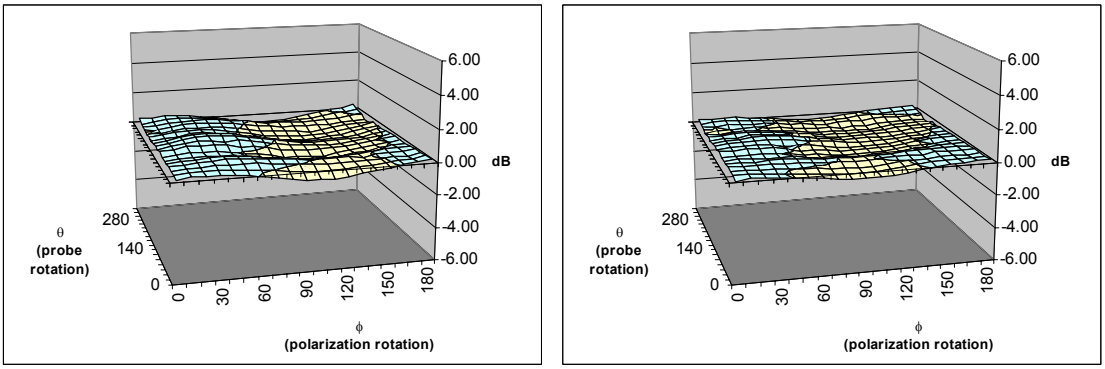

Figure 6: Probe isotropy at 900MHz with probe oriented at 90 degrees to field gradient direction. At left, uncorrected readings. At right, corrected for sensor displacement.

email: enquiries@indexsar.com http://www.indexsar.com
Oakfield House, Cudworth Lane, Newdigate, Surrey, RH5 5BG, UK.

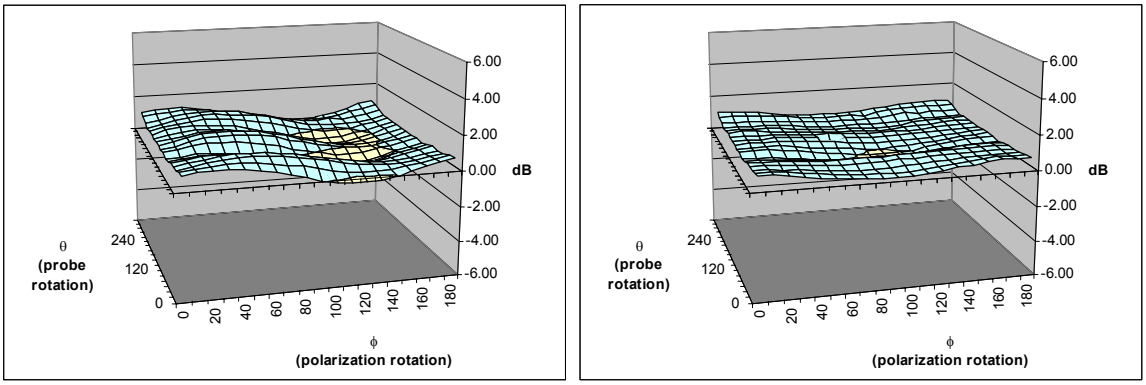

Figure 7: Probe isotropy at 1800MHz with probe oriented at 90 degrees to field gradient direction. At left, uncorrected readings. At right, corrected for sensor displacement.

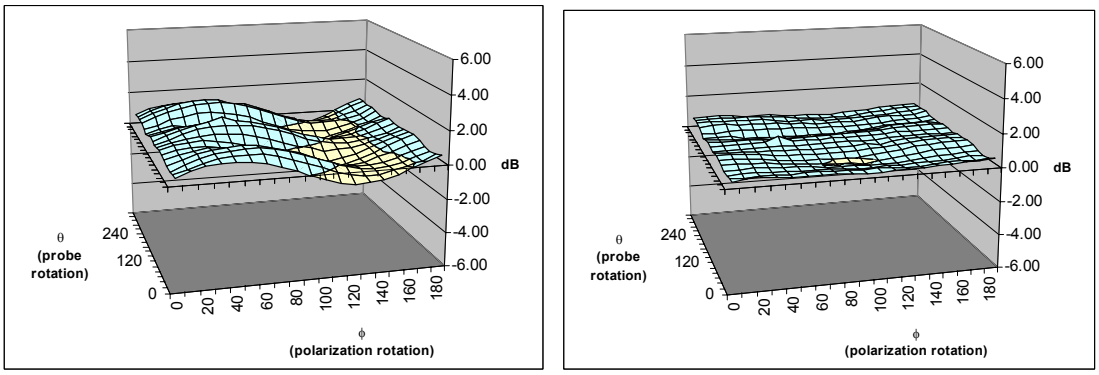

Figure 8: Probe isotropy at 2450MHz with probe oriented at 90 degrees to field gradient direction. At left, uncorrected readings. At right, corrected for sensor displacement.

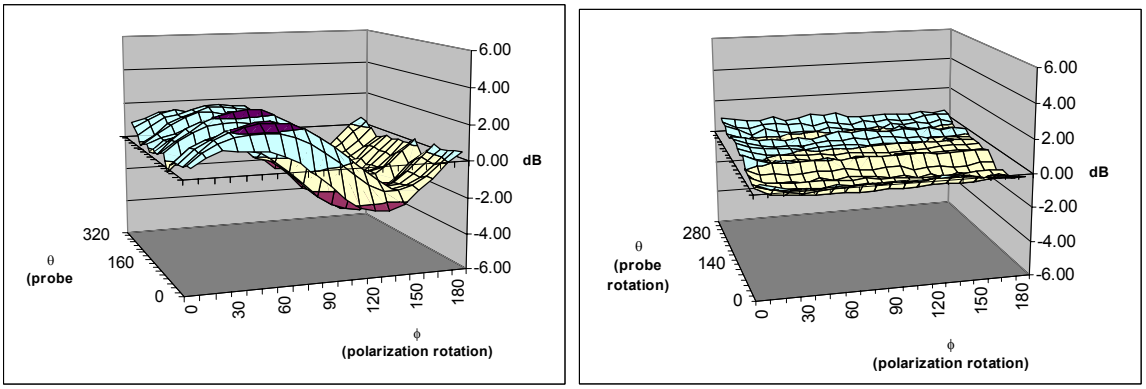

Figure 9: Probe isotropy at 5250MHz with probe oriented at 90 degrees to field gradient direction. At left, uncorrected readings. At right, corrected for sensor displacement. ***Note:*** *dipole used was not dimensioned according to new draft Annex X recommendation for P1528. Additionally, deficiencies in the bearing used to rotate the probe during testing are thought to be the reason for much of the residual variability in the right-hand plot.*

email: enquiries@indexsar.com http://www.indexsar.com
Oakfield House, Cudworth Lane, Newdigate, Surrey, RH5 5BG, UK.

3D scheme for boundary effects correction

The framework introduced above for sensor offsets corrections provides a good foundation for the implementation of an omni-directional boundary effects correction scheme. The starting point for this is the magnitude of the boundary effect error that is deduced from waveguide probe calibration measurements. A typical uncorrected waveguide centerline profile fitted to analytical expectations without correction is shown in Figure 10.

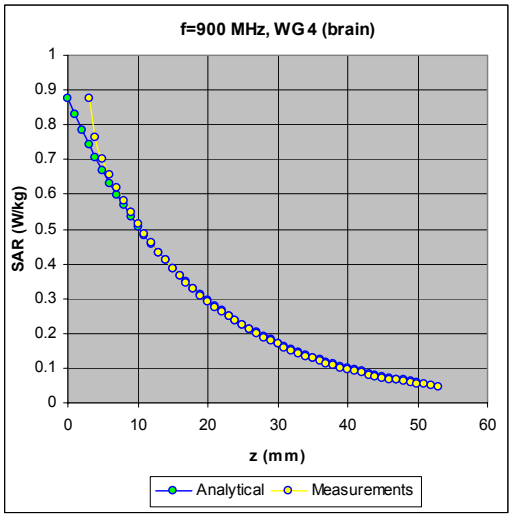

Figure 10: 900MHz waveguide measurement without boundary correction

The following correction implements a satisfactory correction scheme for the waveguide measurements as illustrated in Figure 11, where the correction equation has been applied

$$S_{corr} = S * (1-alpha*EXP(-x/d))$$

where S_{corr} is the SAR measurement corrected for the boundary effect, S is the uncorrected SAR reading, alpha is the correction term for the surface value overestimation and d is the influence depth over which the effect arises. x is the sensor depth from the phantom surface within the lossy liquid.

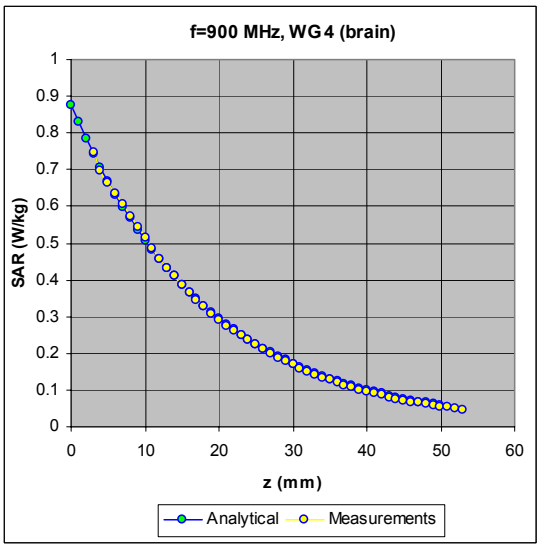

Figure 11: 900MHz waveguide measurement with boundary correction

email: enquiries@indexsar.com http://www.indexsar.com
Oakfield House, Cudworth Lane, Newdigate, Surrey, RH5 5BG, UK.

This correction is basically required because of a geometrically-related influence as the probe approaches the surface and this is supported by measurements, which show a relative insensitivity of the correction factors to frequency or liquid properties. For the Indexsar probes tested, values of alpha=0.65 and d=2mm provide most of the correction required at all frequencies tested and for brain and body liquids.

In the SAR measurement situation with the VPM correction scheme implemented, the probe orientation with respect to the co-ordinate system used for scanning is known and the position and orientation of the phantom surface are also known. The probe orientation has already been used at each point to compute the adjusted sensor positions in 3D and so it is straightforward to apply a separate boundary proximity correction for each sensor based on this information.

There are issues associated with this convenient, procedural approach. Boundary corrections may be thought to be less necessary when the curved side of a probe is brought against a phantom surface compared to the situation of end-on presentation as in a waveguide when all the lossy-liquid is squeezed out at the point of contact. Also, waveguide-determined correction factors are not necessarily applicable to thin-walled phantoms because the thickness and relative permittivity of the liquid barrier are radically different in each case. So, boundary correction schemes probably require a fair amount of further study. Separate corrections for each of the three sensors would seem to be a necessary part of a general correction algorithm and have been implemented in the latest SARA2 software. The success or completeness of this approach will only be finally judged after further experience and testing.

Effects of the corrections on measured SAR profiles

To evaluate the magnitude of the VPM and boundary corrections, the corrections have been applied to scans against a balanced 1800MHz dipole placed at the vertical side of a 2mm wall box phantom. The dipole was oriented vertically and also at 45 degrees to the vertical leaning both to the left and to the right. With the dipole to the left, it is approximately parallel to the nearest sensor of the probe tip, whilst when to the right, it approximately normal to the closest dipole. These therefore represent extremes of the polarization influences. In Figures 12 to 14, the effects of the corrections applied to a central profile from the 3D scans are shown. The first correction applied is the full 3D VPM scheme, where the field gradients are deduced from the 3D measured data. The boundary corrections are applied separately to each sensor based on the scheme and factors referred to above.

email: enquiries@indexsar.com http://www.indexsar.com
Oakfield House, Cudworth Lane, Newdigate, Surrey, RH5 5BG, UK.

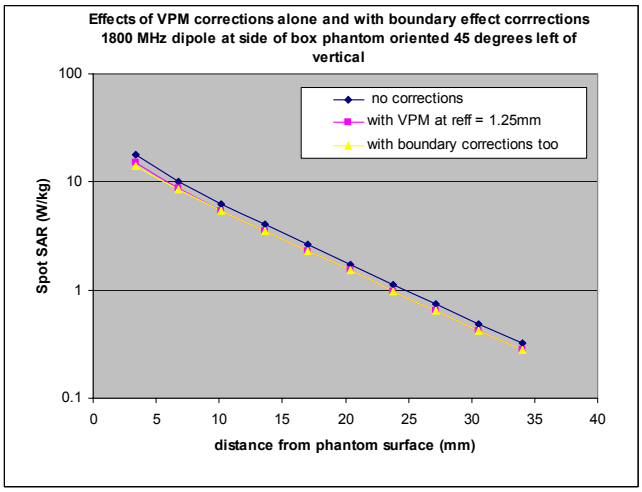

Figure 12: Source dipole oriented approximately parallel to nearest probe sensor

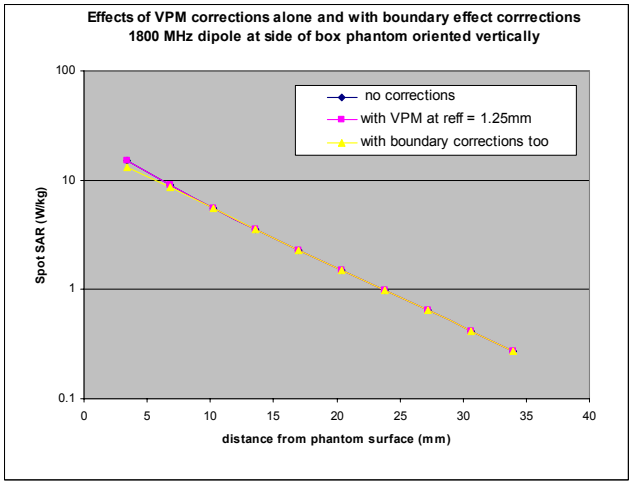

Figure 13: Source dipole oriented vertically (the uncorrected and VPM-corrected lines are essentially co-incident)

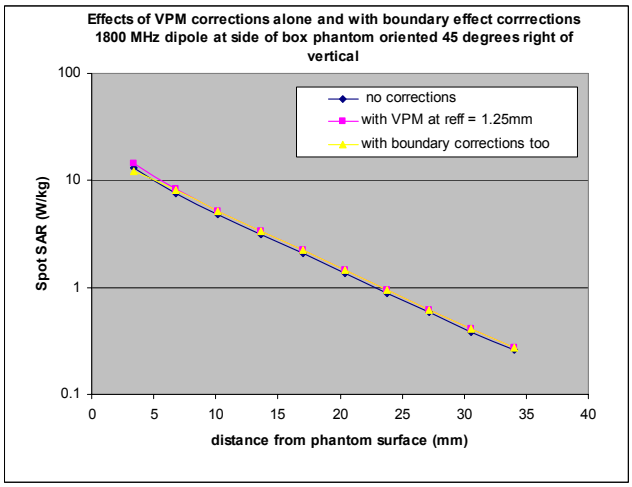

Figure 14: Source dipole oriented approximately normal to nearest probe sensor

email: enquiries@indexsar.com http://www.indexsar.com
Oakfield House, Cudworth Lane, Newdigate, Surrey, RH5 5BG, UK.

Discussion

The analysis presented here shows that even for a SAR probe with 'perfect' geometry and construction, spherical isotropy is unavoidable. When the E-field penetration depth and the tip diameter are comparable, the isotropy range is around +/- 3dB.

The explanation for the analytically-derived isotropy response of probes in field gradients is that the sensor closest to the source is preferentially disposed to overestimating the contribution of fields polarized parallel to the direction of that sensor compared to the contribution of the sensors further away, which have different orientations compared to the applied field polarization. Conversely, the closest sensor is preferentially disposed to underestimating the contribution of fields perpendicular to the direction of that sensor compared to the contribution of the sensors further away. This behaviour introduces a predictable anisotropic response for field orientations that do not align with the probe axis or the plane of its normal. For field polarization directions either normal or perpendicular to the probe axis, the probes retain good isotropy even in field gradients.

The correction procedure proposed in this Report adjusts the values of the field measured by each sensor to make allowance for its actual effective displacement in the field gradient direction compared to where the middle of the probe sensor array is assumed to be. The correction procedure does not require any knowledge of the field polarization direction – just of the field gradient direction.

This process requires that the orientation of the probe and the angular positions of the three sensors within it are known in comparison with the direction of the field gradient. Given this, the displacement of each sensor from the central position can be allowed for if the field gradient is known. The field gradients can be deduced from measured data in a 3D array.

It has been found in this study that the effective displacement of each sensor from the middle position is not given by its physical radius, but is approximately half of the tip radius for the probes investigated. With this established, the corrections for sensor position are simply related to the effective geometrical displacement of each sensor in the direction of the maximum field gradient and to the magnitude of this maximum field gradient.

At 2450MHz the highest frequency (and worst-case) considered within the P1528 range, different schemes for controlling field gradient effects have been compared based on the results obtained as in Table 3.

Table 3: Comparing different schemes for managing SAR probe anisotropy in field gradients at 2450MHz

Reduction scheme	Isotropy range (+/- dB)	Percentage error (+/- %)
None (all angles allowed)	1.136	30
+/- 30 degree constraint	0.844	21
Uni-axial VPM scheme (all angles allowed)	0.789	20
Uni-axial scheme and +/- 40 degree constraint	0.500	12

The implication for upright SAM phantom measurements is that the probe may read low or high at high frequency depending on the source presentation angle. This might most-usually lead to an underestimate at the LH ear (DUT with dipole antenna) but similar overestimate at the RH ear. For the Indexsar probe construction and an upright head, the dipole sensor closest to the surface is in approximate alignment with a handset centerline at the RH ear and approximately normal to it at the LH ear. These effects are small at GSM frequencies, but need correction for higher frequencies – especially over 5GHz.

email: enquiries@indexsar.com http://www.indexsar.com
Oakfield House, Cudworth Lane, Newdigate, Surrey, RH5 5BG, UK.

The VPM correction scheme introduced in this document allows for this and offers comparable or better uncertainty reductions compared to the +/-30 degree constraint proposed in P1528 but without requiring any constraint on probe presentation angles. If used in combination with an angle constraint (see last line of Table 3), much lower uncertainties should be achievable. This correction will certainly need to be applied for any tests >5GHz even with the probe normal but, in any case, lower uncertainties will be achieved by performing measurements at the bottom of a phantom box (for field polarization directions not aligned with the probe axis or its normal).

The box-phantom test geometry used here for isotropy assessment in a field gradient is particularly relevant for upright phantom geometries and provides a realistic assessment of achievable SAR probe isotropy in a field gradient, which is a much more onerous test that that of assessing the isotropy in a uniform field or of reporting solely the rotational isotropy where the direction of field decay is conveniently arranged to align with the probe axis direction (this orientation, widely used for probe calibration, is a unique configuration whereby all three sensors are equally far removed from the source. But any measured SAR distribution will contain field gradients of arbitrary direction and probe anisotropy in response to changing field directions must be considered. This requirement is equally true for probes held perpendicular to the phantom surface as for any other probe presentation geometry (i.e. it is nothing particularly specific to the upright phantom geometry but affects flat-bath measurements as well).

It has been shown that that the isotropy of an immersed SAR E-field probe having traditionally-arranged sensors (on a triangular core) in a field gradient is the same as that in a uniform field when the applied field polarization direction aligns with either the probe axis direction or is normal to the probe axis direction.

Indexsar have frequently reported the equivalence of parallel and normal field measurements. Results have been presented in several Indexsar Reports [2, 3, 4]. These studies compared results obtained from performing scans with the source both at the side of a box phantom (upright geometry) and at the bottom of a box (horizontal geometry). Results from both measurement configurations have been shown to be equivalent. At the side of the box, both horizontal and vertical field polarizations were compared and found to give equivalent results.

The conclusions of these previous studies [2, 3, 4] remain. This new study expands the previous assessments to other field polarisation angles that do not necessarily align with the probe axis or the plane of its normal – a situation that applies in normal device measurement.

With Indexsar IXP-050 probes, the tip casing is of 5mm diameter, but the dipole sensors are interleaved, with the objective of getting the physical centers of the diode-loaded sensors closer together. This study suggests that interleaving the sensors is reducing the effective size of the probe.

The use of the VPM technique described substantially reduces the effective size of the SAR probes over the P1528 frequency range. At frequencies between 5-6GHz, the surface SAR value decays to 1/e of its value in a depth of only 2-3mm. Whilst VPM corrections can reduce the (otherwise large) isotropy range of 5mm probes, the sensor-tip separation distance is such that substantial measurement extrapolations are required for volume averaging. It is anticipated that both smaller probes and the application of VPM would be needed to reduce the isotropy range.

Conclusions

1) The recommendation in P1528 that spherical isotropy range should be determined using angles of incidence from 0 to 90 degrees could potentially lead to only half of the actual spherical isotropy range being collected in the measurements. The theory above shows that it is necessary to perform spherical isotropy measurements over a full 180 degree range (as in Indexsar probe calibrations and as in the tests reported).

email: enquiries@indexsar.com http://www.indexsar.com
Oakfield House, Cudworth Lane, Newdigate, Surrey, RH5 5BG, UK.

2) This study indicates that the effective sensor radius of the orthogonally-arranged sensors in a SAR probe is a characteristic of such probes, which would merit routine determination and reporting.

3) P1528 recommends that probe axis is oriented within +/-30 degrees of the normal to the phantom surface. This requirement could be (and ought to be) more accurately expressed as that the probe axis should be oriented within +/- 30 degrees of the local field gradient. Obviously, the field gradient direction varies with position in any 3D or zoom scan and is not always aligned with the local normal to the phantom surface.

4) The virtual probe miniaturization (VPM) scheme is proposed as an improved technique (compared to +/- 30 degree angle limitations in P1528) that does not require constraint of the probe presentation angle to the local field gradient direction.

5) Existing P1528 recommendations make inadequate distinction between boundary effects and field gradient effects. The field gradient effects, which are dominant, are not related to proximity to the phantom surface, but extend throughout the full measurement range used in SAR testing. Boundary effects will not be fully understood without appreciating field gradient effects.

6) The computational framework needed for corrections of field gradient effects also provide a platform for the correction of boundary effects when the boundary is in an arbitrary direction from the probe axis.

7) The correction procedures proposed can be applied for all systems, where 3-channel SAR probes are used for SAR measurements in 3D.

(VPM corrections as well as an omni-directional probe boundary effect correction scheme have been included in the processing algorithms used by the latest SARA2 software).

Implications for P1528 uncertainty assessment

Table 1 indicates that application of a VPM scheme (as described in this document) is at least as effective in managing probe isotropy uncertainties as is the +/- 30 degree probe presentation angle restriction (to the local phantom surface normal) suggested in P1528. Importantly, this new scheme dispenses with the need for any angle restriction. So, application of a VPM scheme is preferable to a limitation on probe presentation angle. Inspection of figures 3-9 shows that the gradient of probe anisotropy with probe orientation is actually a maximum at the angle of probe normal incidence, so it is not a good idea to rely upon a +/- 30 degrees presentation criterion. Without correction, probe anisotropy is still significant in field gradients to an extent dependent upon frequency. The errors involved for +/- 30 degrees are simple to determine from the theory presented. Application of the VPM scheme will also help manage (the still significant) errors associated with probes presented within +/- 30 degrees of the local surface normal.

A source of uncertainty in the application of this scheme relates to how well the orientation of the sensors within the probe casing are known in relation to the scanning coordinate system. The sensor angular positions need to be known in relation to a reference mark on the probe casing. This can be established during probe calibration using, for example, an arrangement such as that shown in Figure 1. The variations caused by errors in lining up the reference mark can be determined by applying intentional offsets and examining the variations in the VPM-corrected SAR results.

email: enquiries@indexsar.com http://www.indexsar.com
Oakfield House, Cudworth Lane, Newdigate, Surrey, RH5 5BG, UK.

References

[1] P1528 Recommended practice for determining the peak spatial-average absorption rate (SAR) in the human head from wireless communications devices: Measurement techniques. IEEE Std 1528.

[2] IXS209 Error assessment for probe / interface proximity effects for an upright phantom geometry, Indexsar Report, April 2002.

[3] IXS214 Error assessment for probe / interface proximity effects at 1800MHz, Indexsar Report, September 2002.

[4] IXS215 SARA2 validation testing with CDMA-modulated signals at bottom and side of phantom at 1900MHz, October 2002.

email: enquiries@indexsar.com http://www.indexsar.com
Oakfield House, Cudworth Lane, Newdigate, Surrey, RH5 5BG, UK.

Appendix 1: Effect of sensor displacement from probe axis on spatial resolution

A measurement procedure is recommended in P1528 Section A.6.2 to investigate the effect of sensor displacement on spatial resolution. A sharp field minimum is introduced using parallel and opposed dipoles and the minimum is scanned using the probe. Tests have been performed both at the side and the bottom of a box phantom an Indexsar IXP-050 SAR probe. An Indexsar 1.3mm probe was also used. The recommended configuration is reproduced in Figure A1.1.

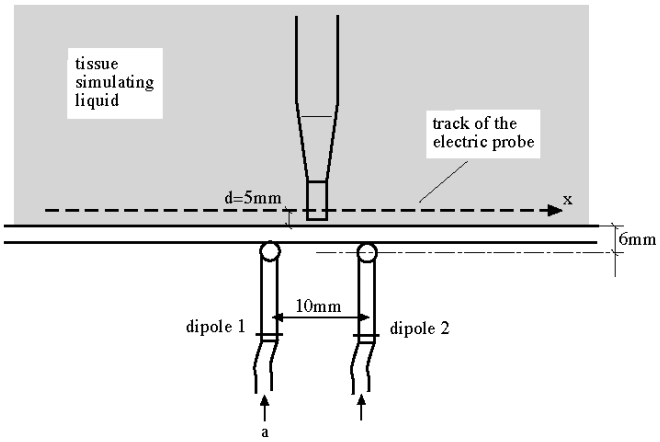

Figure A1.1: Setup used for investigating the behavior of dosimetric probes in normal and strong gradient fields [1]. The dipoles are parallel to each other and orthogonal to the page

This test set-up has been implemented for testing both at the bottom of a box phantom and at the side. The set-up at the side is illustrated in Figure A1.2.

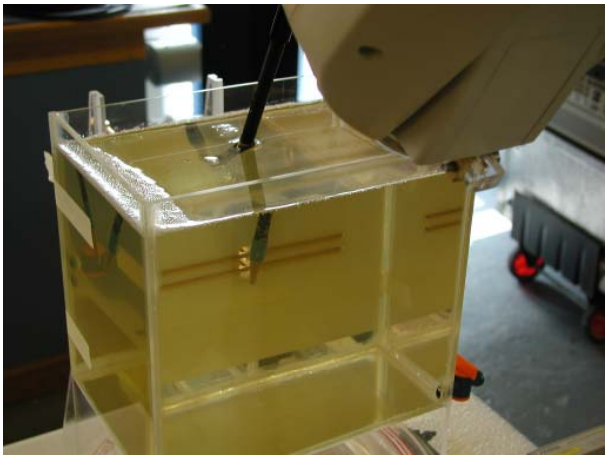

Figure A1.2: Implementation of the test arrangement at the side of a box phantom using 900MHz dipoles

The results obtained by scanning the 1.3mm and 5mm probes across the field minimum between the dipoles are shown in Figure A1.3. A sharper dip is registered at the side of the box for the 5mm probe because the sensor displacements from the plane of the minimum are less in this geometry at the mid-point between the dipoles.

email: enquiries@indexsar.com http://www.indexsar.com
Oakfield House, Cudworth Lane, Newdigate, Surrey, RH5 5BG, UK.

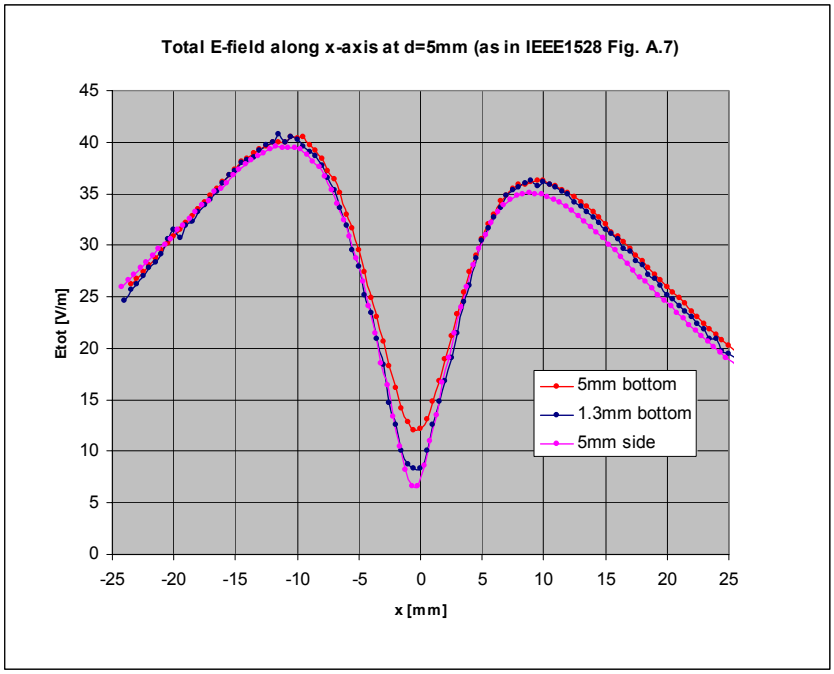

Figure A1.3: Profiles through the dip obtained using measurements every 0.5mm with a 1.3mm probe and with a 5mm probe (see Section A.6 in [1]). For the test done at the side of the box, all the sensors are parallel to the plane of the intended minimum, resulting in better resolution of the minimum and indicating the potential to be realized from sensor offset correction as advanced in this report.

email: enquiries@indexsar.com http://www.indexsar.com
Oakfield House, Cudworth Lane, Newdigate, Surrey, RH5 5BG, UK.

Appendix 2
Outline of steps required of a software algorithm for applying generalized 3D correction algorithm – Virtual Probe Miniaturization (VPM)

1. Make copies of 3D data arrays of raw unlinearized probe output data for each of the three channels.
2. Review each data array prior to processing – zero or negative values may be recorded in the file due to random variability around a notional zero point and these must be addressed. A recommendation is that a zero offset is added to each data point in any array containing values<=0 until the lowest reading is equal to some defined 'floor' of sensitivity. If any of these operations actually need performing on collected data sets, the operations performed need assessing as a percentage error and reporting.
3. Linearise the probe output signals for each channel using appropriate DCPs from the probe calibration data.
4. Evaluate the attenuation constants in each direction for each point of the 3D array.
5. Determine the probe presentation angle and sensor offsets for each measurement point.
6. Compute the correction factors for each point and in each direction.
7. Apply corrections for phantom surface proximity separately for each sensor.
8. Compute the corrected probe outputs for each channel.
9. Apply the probe calibration factors to give results in terms of E or E*E or SAR
10. Report on relevant statistics relating to the VPM conversion to provide assurance that the conversion process has been achieved without introducing anomalies
11. Continue with the remaining post-processing stages.

email: enquiries@indexsar.com http://www.indexsar.com
Oakfield House, Cudworth Lane, Newdigate, Surrey, RH5 5BG, UK.